PHYSICAL REVIEW A **81**, 061802(R) (2010)

Wavelength scaling of efficient high-order harmonic generation by two-color infrared laser fields

Pengfei Lan, Eiji J. Takahashi, and Katsumi Midorikawa
Extreme Photonics Research Group, RIKEN Advanced Science Institute, 2-1 Hirosawa, Wako, Saitama 351-0198, Japan
(Received 8 February 2010; published 25 June 2010)

We theoretically investigate and demonstrate a better wavelength scaling of harmonic yield in a two-color infrared field. By mixing a Ti:sapphire assistant field with the infrared driving field, we show that high harmonic generation is enhanced and the harmonic yield scales as λ^{-3}–λ^{-4} in the plateau region, which falls more slowly as the increase of the driving laser wavelength λ compared with λ^{-5}–λ^{-6} in a one-color infrared field.

DOI: 10.1103/PhysRevA.81.061802 PACS number(s): 42.65.Ky, 42.50.Hz, 32.80.Rm

High-order harmonic generation (HHG) currently provides the most attractive attosecond extreme ultraviolet (XUV) light source [1,2], making a breakthrough in ultrafast optics [1], and also has a broad range of applications in laser physics and photonics (e.g., high-contrast biological imaging and molecular tomography [3]). Increasing the cutoff energy of HHG has been of great interest [4–6], because a broader spectrum enables the generation of shorter attosecond pulses as well as a higher resolution for ultrafast measurement [3]. For the commonly used Ti:sapphire laser (800 nm), a well-known challenge is that the extension of the HHG cutoff is accompanied by an increase of driving laser intensity and ground-state depletion. Whereas high ground-state depletion hinders the enhancement of HHG using the phase-matching technique, by suppressing the ground-state depletion, we can apply not only the right phase matching but also energy scaling [7] to obtain a high-power HHG source. This has motivated the investigations of HHG using infrared (IR) laser pulses [5,6,8–10]. Compared with the Ti:sapphire laser, the longer wavelength IR pulse has several advantages. First, the ponderomotive energy and harmonic cutoff scale as $I\lambda^2$, where I and λ are the driving laser intensity and wavelength, respectively. The harmonic cutoff can be significantly extended by increasing the wavelength while keeping a moderate laser intensity, which also facilitates the phase matching of HHG [6]. Second, the atto-chirp scales as $1/\lambda$ [11]. The longer wavelength IR field enables the generation of shorter attosecond pulses. In this regard, the wavelength scaling of the HHG yield has attracted much more attention [12–19]. However, both the simulations [12–16] and experiments [18,19] demonstrate a rapid drop in the HHG yield as the wavelength increases, which scales unfavorably as λ^{-5}–λ^{-6}. This effect acts one fundamental disadvantage for developing the intense XUV source with an IR driving laser field.

Although the physics underlying the scaling law is more complex [13–15], two factors are considered to lead to the rapid drop in the HHG yield: the spreading of the electron wavepacket, which contributes a factor λ^{-3} [20], and an additional factor λ^{-2} that stems from the distribution of the HHG energy up to the cutoff ($\propto\lambda^2$), although the precise physical origin is not yet fully understood. In other words, the second factor is a cost for the cutoff extension whereas the spreading of the electron wavepacket leads to a "real" decrease in the HHG yield. Therefore, the crucial issue is to suppress the spreading of the electron wavepacket. In this work, we investigate the wavelength scaling of HHG yield in a two-color field with the aim of reducing the rapid drop of the wavelength-dependent HHG yield. By mixing an assistant field with the IR driving pulse, we show that the spreading of the electron wavepacket can be suppressed, then a marked increase and better wavelength scaling of HHG yield can be realized in the two-color IR laser field.

Our scheme is illustrated in Fig. 1. HHG is well explained by a three-step process [21]: The electron is first set free at the ionization time t_i, then travels in the laser field, and finally returns to the parent ion at t_r. Electron excursion includes a leaving process [filled area in Fig. 1(a)] and a returning process [barred area in Fig. 1(a)]. To suppress the electron wavepacket spreading, we propose to mix an assistant field with the main IR pulse. Efficient HHG and the extension of the cutoff require the assistant field to (i) shorten the return time, (ii) boost (or at least not reduce) the ionization rate at the ionization time, and (iii) increase the electron kinetic energy. We can show that the Ti:sapphire laser pulse is the most practically realizable and preferable assistant field that meets these requirements. First the Ti:sapphire laser [dotted line in Fig. 1(a)] reverses its field faster than the IR field [solid line in Fig. 1(a)] and thus assists the IR field in dragging the electron back. Consequently, the return time and electron wavepacket spreading can be reduced. On the other hand, the assistant field enhances the IR field at the ionization time, thus increasing the ionization rate. Moreover, we can show that the maximum kinetic energy in the two-color field E_k^{2c} is approximately proportional to $\alpha I\lambda^2 + \beta I\lambda_{\mathrm{Ti}}^2 + 2\sqrt{\alpha\beta}I\lambda\lambda_{\mathrm{Ti}}$, where αI and βI are the intensities of the IR and Ti:sapphire fields, respectively, and λ and λ_{Ti} are the corresponding wavelengthes, respectively. Compared with that in the one-color IR field E_k^{1c}, which is approximately proportional to $I\lambda^2$, the assistant field induces a cutoff extension, that is, the cross term $2\sqrt{\alpha\beta}I\lambda\lambda_{\mathrm{Ti}}$, in the two-color case. At a fixed intensity, we can show that $E_k^{2c} - E_k^{1c} \propto \beta I\lambda_{\mathrm{Ti}}^2 + 2\sqrt{\alpha\beta}I\lambda\lambda_{\mathrm{Ti}} - \beta I\lambda^2 \approx 2\sqrt{\alpha\beta}I\lambda\lambda_{\mathrm{Ti}} - \beta I\lambda^2 > 0$ as long as $2\sqrt{\alpha/\beta} > \lambda/\lambda_{\mathrm{Ti}}$. Therefore, the cutoff extension can also be achieved in the two-color field. By contrast, we note that the conventional two-color method that combines the fundamental IR field with its second-harmonic assistant field [22] does not fulfill these requirements simultaneously, because the increase of cutoff energy is usually accompanied by a reduction of the ionization rate [4,22].

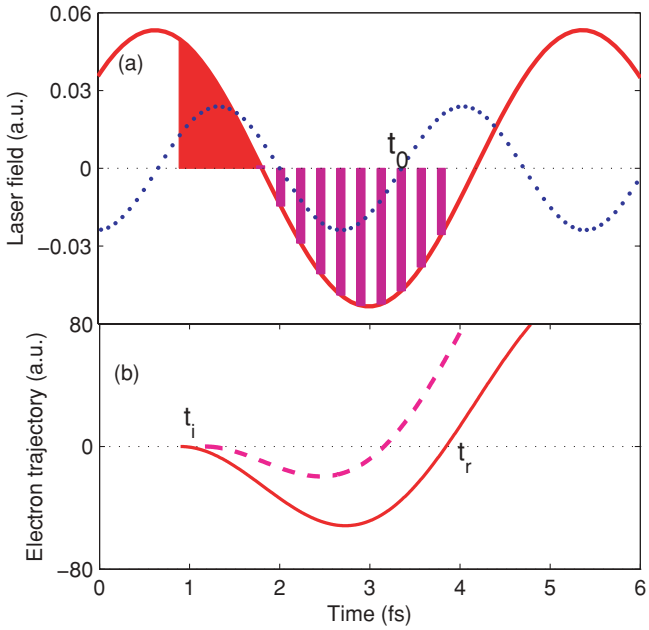

FIG. 1. (Color online) (a) Electric field of 1400-nm IR field (solid line) and 800-nm Ti:sapphire field (dotted line). (b) Classical electron trajectories that correspond to HHG in the plateau (dashed line) and cutoff (solid line) regions.

To demonstrate our scheme, we solve the time-dependent Schrödinger equation (TDSE)

$$i\frac{\partial\psi(\mathbf{r},t)}{\partial t} = \left[-\frac{\nabla^2}{2} + V(r) + zE(t)\right]\psi(\mathbf{r},t), \qquad (1)$$

where $V(r)$ is the atomic potential and atomic units (a.u.) are used. Here, $V(r) = -\frac{1}{r}$ for H and $-[1+\exp(-2.1340r)]/r$ for He and the ionization energies I_p are 13.6 and 24.2 eV, respectively. The linearly polarized electric field is expressed as $E(t) = f(t)[E_{\rm IR}\sin(\omega_{\rm IR}t + \phi_{\rm IR}) + E_{\rm Ti}\sin(\omega_{\rm Ti}t + \phi_{\rm Ti})]$, where $E_{\rm IR,Ti}$, $\omega_{\rm IR,Ti}$, and $\phi_{\rm IR,Ti}$ are the amplitudes, frequencies, and carrier-envelope phases (CEPs) of the IR and Ti:saphire laser fields, respectively. As in Refs. [13,14], $f(t)$ is a trapeziform envelope function corresponding to a nine-cycle flat top with a half-cycle turn-on and turn-off. The wavelength of the IR field changes from 900 to 1800 nm and that of the Ti:sapphire field is 800 nm. $\phi_{\rm Ti} = \phi_{\rm IR} = 0$ in the calculation. The harmonic spectrum is shown in Fig. 2(a) for an IR field of 1400 nm. The laser intensity is 1×10^{14} W/cm^2 and the intensity ratios between the IR and Ti:sapphire laser fields are 10:0 (dashed line, i.e., one-color IR field) and 8:2 (solid line). As shown in Fig. 2(a), the mixing of the assistant field slightly extends the harmonic cutoff. Moreover, several new frequency components, which correspond to the generation of high-order sum and different frequencies [23], are generated in the two-color field, resulting in a dense harmonic spectrum. Such a dense harmonic spectrum also has an advantage for easier generation of continuous harmonics and single attosecond pulses with multicycle laser pulses [24]. Moreover, an increase of the harmonic intensity is achieved in the two-color field excluding the highest five harmonics. Consequently, the HHG yield integrated from 30 to 40 eV is

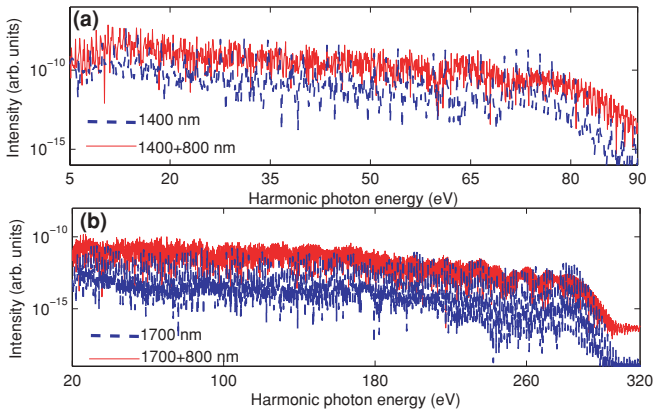

FIG. 2. (Color online) (a) High-order harmonic spectra generated from H at an intensity of 1×10^{14} W/cm^2. The wavelengths of the IR and assistant Ti:sapphire laser are 1400 and 800 nm, respectively. The intensity ratios are 10:0 (dashed line) and 8:2 (solid line). (b) High-order harmonic spectra generated from He at an intensity of 3×10^{14} W/cm^2. The IR wavelength is 1700 nm and intensity ratios are 10:0 (dashed line) and 6:4 (solid line).

increased by a factor of 4 (see Fig. 3) compared with that in the one-color IR field.

The wavelength scaling law is evaluated by integrating the HHG yield from 30 to 40 eV. As shown in Fig. 3(a), the HHG yield scales as $\lambda^{-5.39}$ in the one-color IR field, while a marked enhancement is realized in the two-color field and the wavelength scaling decreases to $\lambda^{-3.4}$ and $\lambda^{-3.3}$ for the intensity ratios of 8:2 and 6:4. To evaluate the scaling law for harmonics at higher photon energies, we use an alternative approach to define the integration region. In this case, the harmonic spectrum is separated into (i) a plateau region that ranges from I_p to $I_p + 1.5U_p$, (ii) a high-plateau region that ranges from $I_p + U_p$ to $I_p + 2U_p$, and (iii) a cutoff region that ranges from $I_p + 2U_p$ to $I_p + 3.17U_p$. Here

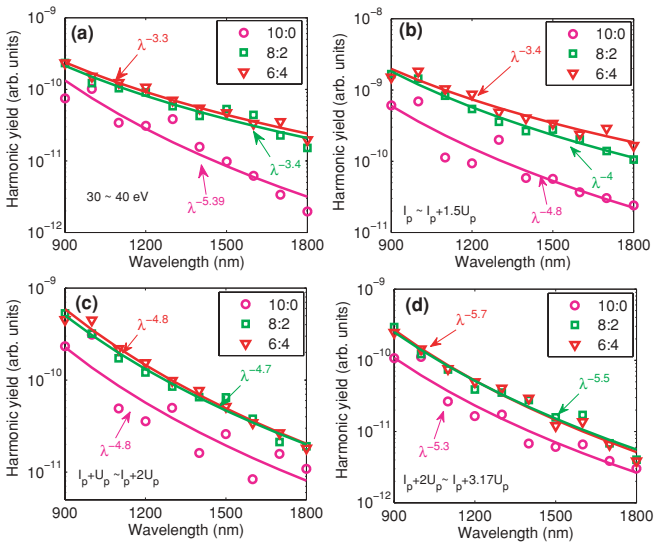

FIG. 3. (Color online) Wavelength scaling of HHG yield integrated over (a) the energy range 30–40 eV, (b) $I_p \sim I_p + 1.5U_p$, (c) $I_p + U_p \sim I_p + 2U_p$, and (d) $I_p + 2U_p \sim I_p + 3.17U_p$. The target is H and the laser intensity is 1×10^{14} W/cm^2.

I_p is the ionization energy of the target atom, U_p [eV] = $9.337 \times 10^{-14} I$ [W/cm^2](λ [μm])^2 is the ponderomotive energy, and $I = 1 \times 10^{14}$ is the total laser intensity. Note that the integration region in this approach increases as the IR wavelength increases. The scaling laws of HHG yield in the plateau, high-plateau, and cutoff regions are shown in Figs. 3(b), 3(c), and 3(d), respectively. Compared with the one-color case, a better wavelength scaling law of λ^{-3}–λ^{-4} is achieved for plateau harmonics in the two-color field and the HHG yield is also significantly enhanced. However, the scaling law becomes $\lambda^{-4.8}$ in the high-plateau region, which is similar to the one-color case, and $\lambda^{-5.7}$ in the cutoff region. Although an unfavorable scaling law is still shown in the cutoff region, the HHG yield is enhanced in the two-color field and is about twice as high as that in the one-color case. These results clearly show that the mixing of the assistant pulse with the IR field has an advantage both for extending the cutoff energy and enhancing the HHG yield.

To confirm the better wavelength scaling at higher laser intensities and photon energies, we calculate the high-order harmonics generated from He. The laser intensity is increased to 3×10^{14} W/cm^2. The harmonic spectra are shown in Fig. 2(b) for the one-color field (dashed line) and two-color field (solid line), respectively. One can see that the cutoff energy reaches 300 eV and the HHG yield is significantly increased in the two-color case except for the harmonics ranging from 280 to 290 eV. The wavelength scaling of the HHG yield integrated from 30 to 100 eV is shown in Fig. 4(a). Similar to the HHG at lower intensity [see Fig. 3(a)], Fig. 4(a) clearly shows an increase of HHG yield in the two-color field and also indicates a better scaling law. We also evaluate the HHG yield in the plateau, high-plateau, and cutoff regions and the results are shown in Figs. 4(b), 4(c), and 4(d), respectively. Note that this approach involves the influence of target dependence [17]. Therefore, a slight quantitative difference between the scaling laws of H and He can be seen by comparing Figs. 4 with 3. However, as shown by Fig. 4, a better scaling still can be realized in the two-color case except for the high harmonics in the cutoff region.

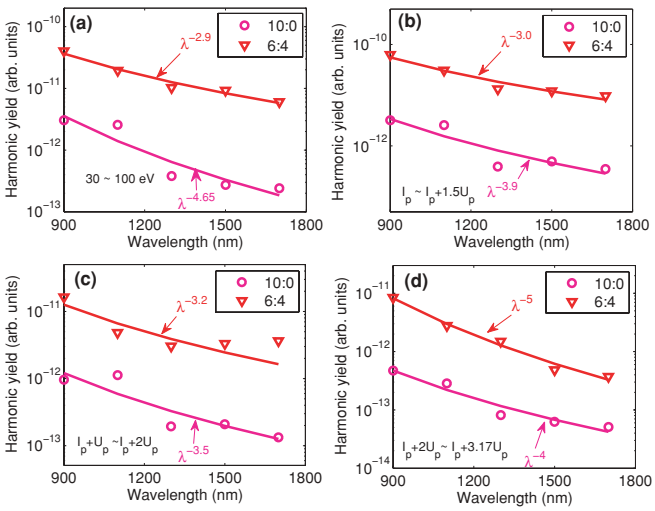

FIG. 4. (Color online) Same to Fig. 3, but for He and a higher laser intensity of 3×10^{14} W/cm^2.

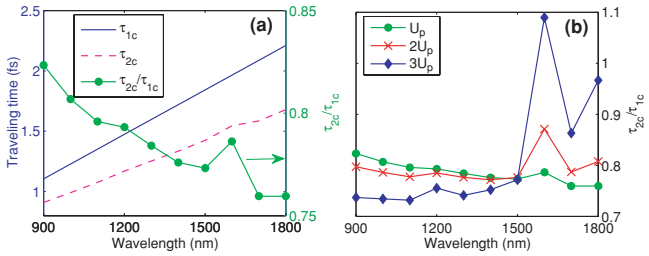

FIG. 5. (Color online) (a) Traveling time for the recombination energy of U_p in the two-color and one-color fields and their ratio τ_{2c}/τ_{1c}. (b) The traveling time ratio τ_{2c}/τ_{1c} for the recombination energies of U_p, $2U_p$, and $3U_p$, respectively. The intensity ratio is 8:2.

A deeper insight into the scaling law can be achieved by taking account of the spread of electron wavepacket according to the three-step model [21]. By considering a Gaussian wavepacket with an initial width a_0 at the ionization time, the wavepacket width $a(\tau)$ after traveling a time τ can be given by [25]

$$a(\tau)^2 = a_0^2 + \tau^2 / a_0^2. \tag{2}$$

The initial width $a_0 \approx 4.3$ a.u. in the strong-field approximation [25]. We also preform a simulation with TDSE and a_0 is calculated to be 6 a.u. The traveling time is calculated with the three-step model [21] for the electron trajectory that corresponds to the kinetic energy of U_p (plateau region) in the one-color (τ_{1c}) and two-color (τ_{2c}) fields. Note that two classical trajectories contribute to HHG in the plateau region. The results shown in Fig. 5 correspond to the short trajectory, which induces a smaller wavepacket spreading compared with the long trajectory and is preferably selected in experiments. As shown in Fig. 5(a), the traveling time in the two-color field is reduced ($\tau_{2c}/\tau_{1c} \sim 0.8$) and increases more slowly with increasing wavelength, which consequently slows down the wavepacket spreading. We also calculate the long trajectory. Our calculation shows that, compared with the short trajectory, the two-color field induces a weaker influence on the long trajectory ($\tau_{2c}/\tau_{1c} \sim 0.9$) and the traveling time increases similarly in the two-color and one-color fields. Therefore we focus on the short trajectory in the following discussion.

Upon substitution of the traveling time into Eq. (2), the scaling of electron wavepacket widths are calculated to be $\lambda^{0.92}$ and $\lambda^{0.6}$ in the one-color and two-color fields, respectively, and thus the wavepacket spreading approximately contributes factors of $\lambda^{-2.8}$ and $\lambda^{-1.8}$ to the scaling law. By including the additional factor λ^{-2} due to the cutoff extension, the scaling law of the HHG yield is estimated to be $\lambda^{-4.8}$ and $\lambda^{-3.8}$ in the one-color and two-color fields, respectively. Therefore, a better scaling law is obtained for the plateau harmonics in the two-color field, which agrees with the simulation based on TDSE. For comparison, we consider the HHG in the cutoff region; the corresponding electron trajectory is shown in Fig. 1(b) (solid line). Obversely, the traveling time is longer than the trajectory in the plateau region. In this case, the assistant field reverses its direction at t_0 prior to the recombination and the following field (from t_0 to t_r) hinders the electron's return. This effect is negligible for a shorter IR wavelength. However,

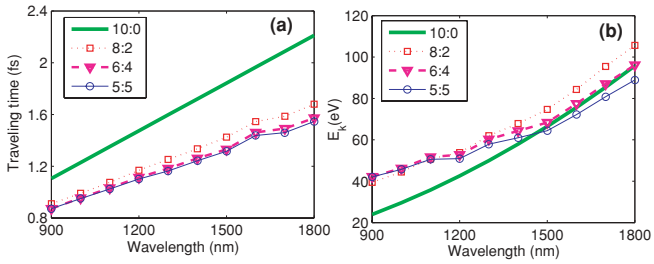

FIG. 6. (Color online) (a) Traveling time of the electron trajectory that corresponds to the recombination energy of U_p. (b) The maximum kinetic energy at the recombination time.

it gradually increases with increasing IR wavelength and traveling time. Therefore, as shown in Fig. 5(b), the traveling time ratio between the two-color and one-color fields, τ_{2c}/τ_{1c} (solid, diamond line), increases with wavelength. According to Eq. (2), this effect leads to an increase of wavepacket spreading and a faster drop of HHG yield in the cutoff region. It should be noted that the assistant field near t_0 is very weak and does not significantly increase the traveling time; τ_{2c} is still shorter than τ_{1c}. Also the ionization rate is enhanced in the two-color field. Therefore a higher harmonic yield still is achieved in the two-color case. The electron trajectory corresponding to HHG in the high-plateau region is also calculated, which shows that τ_{2c}/τ_{1c} changes slightly and therefore results in a similar scaling law in the two-color and one-color fields. These features explain qualitatively the scaling law obtained from the simulation of TDSE.

Finally, we consider optimizing the intensity ratio between the IR and Ti:sapphire laser pulses. As shown in Fig. 6(a), the traveling time and thus wavepacket spreading can be suppressed by increasing the Ti:sapphire laser intensity. However, the cutoff extension $E_k^{2c} - E_k^{1c} \propto (2\sqrt{\alpha/\beta} - \lambda/\lambda_{\mathrm{Ti}})$ is reduced when increasing the Ti:sapphire laser intensity. As shown in Fig. 6(b), E_k^{2c} becomes lower than E_k^{1c} for $\lambda > 1500$ nm when the intensity ratio is less than 5:5. Therefore, an optimized intensity ratio around 6:4 enables one to efficiently suppress the wavepacket spreading without reducing the cutoff energy. We also calculated the CEP dependence by changing ϕ_{IR} (or ϕ_{Ti}) but fixing $\phi_{\mathrm{Ti}} = 0$ (or $\phi_{\mathrm{IR}} = 0$), which shows that the traveling time and cutoff energy are insensitive to the CEP of two-color fields.

In conclusion, we theoretically investigated and demonstrated a marked enhancement and a better wavelength scaling of harmonic yield by mixing a Ti:sapphire assistant field with the IR driving field. Moreover, the cutoff energy in the two-color field is shown to be also higher than that in the one-color field. Thus the two-color IR field provides a better method toward the efficient generation of XVU light sources with high photon energies.

P.F.L. is grateful to The Foreign Postdoctoral Researcher (FPR) Program of RIKEN.

[1] M. Hentschel *et al.*, Nature (London) **414**, 509 (2001).
[2] P. M. Paul *et al.*, Science **292**, 1689 (2001).
[3] J. Itatani *et al.*, Nature (London) **432**, 867 (2004).
[4] L. Chipperfield, J. J. Robinson, J. W. G. Tisch, and J. P. Marangos, Phys. Rev. Lett. **102**, 063003 (2009).
[5] B. Shan and Z. Chang, Phys. Rev. A **65**, 011804(R) (2001).
[6] E. J. Takahashi *et al.*, Phys. Rev. Lett. **101**, 253901 (2008).
[7] E. J. Takahashi *et al.*, Phys. Rev. A **66**, 021802(R) (2002).
[8] T. Popmintchev *et al.*, Opt. Lett. **33**, 2128 (2008).
[9] C. Vozzi *et al.*, Phys. Rev. A **79**, 033842 (2009).
[10] F. Calegari *et al.*, Opt. Lett. **34**, 3125 (2009).
[11] G. Doumy *et al.*, Phys. Rev. Lett. **102**, 093002 (2009).
[12] J. Tate *et al.*, Phys. Rev. Lett. **98**, 013901 (2007).
[13] K. Schiessl *et al.*, Phys. Rev. Lett. **99**, 253903 (2007).
[14] K. Ishikawa *et al.*, Phys. Rev. A **79**, 033411 (2009).
[15] K. Ishikawa *et al.*, Phys. Rev. A **80**, 011807(R) (2009).
[16] M. V. Frolov *et al.*, Phys. Rev. Lett. **100**, 173001 (2008).
[17] M. V. Frolov *et al.*, Phys. Rev. Lett. **102**, 243901 (2009).
[18] P. Colosimo *et al.*, Nature Phys. **4**, 386 (2008).
[19] A. D. Shiner *et al.*, Phys. Rev. Lett. **103**, 073902 (2009).
[20] M. Lewenstein *et al.*, Phys. Rev. A **49**, 2117 (1994).
[21] P. B. Corkum, Phys. Rev. Lett. **71**, 1994 (1993).
[22] C. Faria *et al.*, Phys. Rev. A **61**, 063415 (2000); **60**, 1377 (1999); T. Pfeifer *et al.*, Phys. Rev. Lett. **97**, 163901 (2006).
[23] M. D. Perry and J. K. Crane, Phys. Rev. A **48**, R4051 (1993).
[24] E. J. Takahashi *et al.*, Phys. Rev. Lett. **104**, 233901 (2010).
[25] B. Gottlieb *et al.*, Phys. Rev. A **54**, R1022 (1996).